

Chapter 4

The Continuum Model for Planar Arrays

As described in Section 2.6, coupled oscillator arrays can be constructed in a planar geometry in which each oscillator is coupled to more than the two nearest neighbors of the linear array case. In that section a Cartesian coupling topology is described in which each oscillator is coupled to four nearest neighbors, and the array boundary is rectangular. In such an arrangement, the phase distributions suitable for beam-steering are obtainable either by detuning the edge oscillators [42] or by injecting them with external signals with adjustable phase [43]. Both of these approaches are treatable via the continuum model. Further generalizing the planar arrangement, one may use alternative coupling topologies such as the triangular lattice in which each oscillator is coupled to six nearest neighbors and the array boundary is triangular or the hexagonal lattice in which each oscillator is coupled to three nearest neighbors and the array boundary is again triangular [44] [45]. As will be shown in this chapter, these coupling topologies are also treatable using the continuum model.

4.1 Cartesian Coupling in the Continuum Model without External Injection

We begin with Eq. (2.6-3) for a $2M + 1$ by $2N + 1$ rectangular array with zero coupling phase replacing the discrete indices i and j with the continuous variables x and y , respectively; and we expand the phase function in a two-dimensional Taylor series retaining terms to second order. By this process, we obtain the two-dimensional analog of Eq. (3.1-3); that is,

$$\frac{d\varphi}{d\tau} = \left(\frac{\omega_0(x, y, \tau) - \omega_{ref}}{\Delta\omega_{lock}} \right) + \frac{\partial^2 \varphi}{\partial x^2} + \frac{\partial^2 \varphi}{\partial y^2} \quad (4.1-1)$$

or

$$\frac{\partial^2 \varphi}{\partial x^2} + \frac{\partial^2 \varphi}{\partial y^2} - \frac{d\varphi}{d\tau} = -\Delta\Omega_{tune} \quad (4.1-2)$$

subject to Neumann boundary conditions at the array edges. (These boundary conditions may be ascertained via the fictitious additional oscillator artifice described in Section 3.1.) Averaging Eq. (4.1-2) over the two dimensional array and using the boundary conditions as in Eqs. (3.1-9) to (3.1-13), it can be shown that the ensemble frequency of the array is the average of the tuning (free running) frequencies of the oscillators.

Laplace transformation of Eq. (4.1-2) with respect to the scaled time, τ , results in,

$$\frac{\partial^2 \tilde{\varphi}}{\partial x^2} + \frac{\partial^2 \tilde{\varphi}}{\partial y^2} - s\tilde{\varphi} = -\Delta\tilde{\Omega}_{tune} \quad (4.1-3)$$

where the tilde denotes the transformed function. As in the one-dimensional case, this equation can be solved by postulating a solution as a sum of eigenfunctions of the two-dimensional differential operator, the Laplacian operator, and solving for the coefficients of this expansion. As indicated in [42], the eigenfunctions are,

$$\begin{aligned} f_{ee,mn} &= \frac{1}{N_{ee,mn}} \cosh(\sqrt{s_m} x) \cosh(\sqrt{s_n} y) \\ f_{oo,kl} &= \frac{1}{N_{oo,kl}} \sinh(\sqrt{s_k} x) \sinh(\sqrt{s_l} y) \\ f_{eo,m\ell} &= \frac{1}{N_{eo,m\ell}} \cosh(\sqrt{s_m} x) \sinh(\sqrt{s_\ell} y) \\ f_{oe,kn} &= \frac{1}{N_{oe,kn}} \sinh(\sqrt{s_k} x) \cosh(\sqrt{s_n} y) \end{aligned} \quad (4.1-4)$$

where the eigenvalues are,

$$\begin{aligned}
 s_k &= -\left(\frac{(2k+1)\pi}{2a+1}\right)^2 & s_m &= -\left(\frac{2m\pi}{2a+1}\right)^2 \\
 s_\ell &= -\left(\frac{(2\ell+1)\pi}{2b+1}\right)^2 & s_n &= -\left(\frac{2n\pi}{2a+1}\right)^2
 \end{aligned}
 \tag{4.1-5}$$

and the normalization constants are,

$$\begin{aligned}
 N_{ee,mn} &= \frac{1}{2}\sqrt{(2a+1)(2b+1)\eta_m\eta_n} \\
 N_{oo,kl} &= \frac{1}{2}\sqrt{(2a+1)(2b+1)} \\
 N_{ee,m\ell} &= \frac{1}{2}\sqrt{(2a+1)(2b+1)\eta_m} \\
 N_{oo,kn} &= \frac{1}{2}\sqrt{(2a+1)(2b+1)\eta_n}
 \end{aligned}
 \tag{4.1-6}$$

where,

$$\eta_m = \begin{cases} 2; & m = 0 \\ 1; & m \neq 0 \end{cases}
 \tag{4.1-7}$$

The general solution procedure follows that used in the case of the linear array. That is, we postulate a two dimensional delta function source to obtain the Green's function as an expansion in the two dimensional eigenfunctions. Then, we integrate the product of this Green's function and the actual source function over the array to obtain the phase distribution as an expansion in the eigenfunctions. This solution is presented in Ref. [42].

The Green's function, $\tilde{g}(x, y, x', y', s)$, is a solution of,

$$\frac{\partial^2 \tilde{g}}{\partial x^2} + \frac{\partial^2 \tilde{g}}{\partial y^2} - s\tilde{\varphi} = -\delta(x-x')\delta(y-y')
 \tag{4.1-8}$$

The solution of this equation expressed as a sum of eigenfunctions is,

$$\begin{aligned}
g_{\tilde{z}} &= \sum_{n=0}^{\infty} \sum_{m=0}^{\infty} \frac{f_{ee,mn}(x', y') f_{ee,mn}(x, y)}{s_m + s_n - s} \\
&+ \sum_{\ell=0}^{\infty} \sum_{k=0}^{\infty} \frac{f_{oo,k\ell}(x', y') f_{oo,k\ell}(x, y)}{s_k + s_{\ell} - s} \\
&+ \sum_{\ell=0}^{\infty} \sum_{m=0}^{\infty} \frac{f_{eo,m\ell}(x', y') f_{eo,m\ell}(x, y)}{s_m + s_{\ell} - s} \\
&+ \sum_{n=0}^{\infty} \sum_{k=0}^{\infty} \frac{f_{oe,kn}(x', y') f_{ee,mn}(x, y)}{s_k + s_n - s}
\end{aligned} \tag{4.1-9}$$

This Green's function can then be multiplied by the detuning function, $\Delta\tilde{\Omega}_{tune}(x', y', s)$, and integrated over the array. The inverse Laplace transform is easily obtained as the sum of the residues at the poles as in the one dimensional case. Recall that the detuning of the oscillators required to produce a desired phase distribution across the array can be determined by merely substituting the desired phase distribution into Eq. (4.1-2). From the theory of uniformly spaced phased array antennas, the steady-state phase distribution necessary to produce a beam steered to spherical coordinate angles, θ_0, φ_0 , with the polar axis normal to the plane of the array, is

$$\varphi_{ss}(x, y) = \frac{\Omega_x}{2} (|x+a| - |x-a|) + \frac{\Omega_y}{2} (|y+b| - |y-b|) \tag{4.1-10}$$

where,

$$\begin{aligned}
\Omega_x &= -2\pi \frac{h}{\lambda} \sin \theta_0 \cos \varphi_0 \\
\Omega_y &= -2\pi \frac{h}{\lambda} \sin \theta_0 \sin \varphi_0
\end{aligned} \tag{4.1-11}$$

and h is the element spacing while λ is the wavelength. Substituting into Eq. (4.1-2) with the time derivative set to zero to obtain the steady-state result, we find that,

$$\Delta\Omega_{tune} = -\Omega_x [\delta(x+a) - \delta(x-a)] - \Omega_y [\delta(y+b) - \delta(y-b)] \tag{4.1-12}$$

Thus, we discover that beam-steering requires detuning of only the edge oscillators and that the needed detuning is constant along each edge. This leads us to seek dynamic solutions of Eq. (4.1-2) that result from a temporal step detuning of the edge oscillators that is constant along each edge. That is, we limit ourselves to detuning functions of the general form,

$$\Delta\Omega_{tune} = \Omega_{x1}\delta(x+a)u(\tau) + \Omega_{x2}\delta(x-a)u(\tau) + \Omega_{y1}\delta(y+b)u(\tau) + \Omega_{y2}\delta(y-b)u(\tau) \quad (4.1-13)$$

For step temporal dependence, the Laplace transform of the detuning is,

$$\Delta\tilde{\Omega}_{tune} = \frac{\Omega_{x1}}{s}\delta(x+a) + \frac{\Omega_{x2}}{s}\delta(x-a) + \frac{\Omega_{y1}}{s}\delta(y+b) + \frac{\Omega_{y2}}{s}\delta(y-b) \quad (4.1-14)$$

The presence of the delta functions facilitates integration of the product of the Green's function and the tuning function leading to the solution.

$$\begin{aligned} \varphi(x, y, \tau) = & \left(\frac{\Omega_{x1} + \Omega_{x2}}{2a+1} + \frac{\Omega_{y1} + \Omega_{y2}}{2b+1} \right) \tau u(\tau) \\ & + \frac{1}{2a+1} \sum_{p=1}^{\infty} \frac{\left(\Omega_{x1} + (-1)^p \Omega_{x2} \right) \cos\left(\frac{p\pi}{2a+1}(x+a) \right)}{\left(\frac{p\pi}{2a+1} \right)^2} \left(1 - e^{-\left(\frac{p\pi}{2a+1} \right)^2 \tau} \right) u(\tau) \\ & + \frac{1}{2a+1} \sum_{p=1}^{\infty} \frac{\left((-1)^p \Omega_{x1} + \Omega_{x2} \right) \cos\left(\frac{p\pi}{2a+1}(x-a) \right)}{\left(\frac{p\pi}{2a+1} \right)^2} \left(1 - e^{-\left(\frac{p\pi}{2a+1} \right)^2 \tau} \right) u(\tau) \\ & + \frac{1}{2b+1} \sum_{p=1}^{\infty} \frac{\left(\Omega_{y1} + (-1)^p \Omega_{y2} \right) \cos\left(\frac{p\pi}{2b+1}(x+b) \right)}{\left(\frac{p\pi}{2b+1} \right)^2} \left(1 - e^{-\left(\frac{p\pi}{2b+1} \right)^2 \tau} \right) u(\tau) \\ & + \frac{1}{2b+1} \sum_{p=1}^{\infty} \frac{\left((-1)^p \Omega_{y1} + \Omega_{y2} \right) \cos\left(\frac{p\pi}{2b+1}(x-b) \right)}{\left(\frac{p\pi}{2b+1} \right)^2} \left(1 - e^{-\left(\frac{p\pi}{2b+1} \right)^2 \tau} \right) u(\tau) \end{aligned} \quad (4.1-15)$$

which is the solution for the special case of constant detuning along each edge of the array. In steady state, this reduces to Fourier series that can be summed in closed form resulting in,

$$\begin{aligned}
 \varphi(x, y, \tau) = & \left(\frac{\Omega_{x1} + \Omega_{x2}}{2a+1} + \frac{\Omega_{y1} + \Omega_{y2}}{2b+1} \right) \tau \\
 & + \left[\frac{\Omega_{x1} + \Omega_{x2}}{2} \right] \left[\frac{2a+1}{6} + \frac{a^2 + x^2}{2a+1} - (|x+a| + |x-a|) \right] \\
 & - \left[\frac{\Omega_{x1} - \Omega_{x2}}{2} \right] \left[(|x+a| - |x-a|) \right] \\
 & + \left[\frac{\Omega_{y1} + \Omega_{y2}}{2} \right] \left[\frac{2b+1}{6} + \frac{b^2 + y^2}{2b+1} - (|y+b| + |y-b|) \right] \\
 & - \left[\frac{\Omega_{y1} - \Omega_{y2}}{2} \right] \left[(|y+b| - |y-b|) \right]
 \end{aligned} \tag{4.1-16}$$

which clearly shows that symmetric detuning gives rise to parabolic steady-state phase distributions whereas antisymmetric detuning results in linear steady-state phase distributions. In the antisymmetric case where $\Omega_{x1} = -\Omega_{x2} = -\Omega_x$ and $\Omega_{y1} = -\Omega_{y2} = -\Omega_y$, Eq. (4.1-16) reduces to Eq. (4.1-10).

The phase distribution as function of time for beam-steering to 10 deg of polar angle at -110 deg of azimuth as given by Eq. (4.1-15) is shown in Fig. 4-1. Note that during the transient, the phase distribution is not planar, but in steady state at infinite time it becomes planar. Figure 4-2 shows the beam peak and 3-dB contour of the far-zone radiated field of a half-wavelength spaced array of isotropic radiating elements excited by this two-dimensional oscillator array during the transient period at intervals of 10 inverse locking ranges. Because the phase during the transient is not planar, the directivity of the antenna is decreased. Assuming no losses, the gain is equal to this directivity. The gain is plotted as a function of time in Fig. 4-3 and compared with the ideal gain were the phase planar. The gain reduction observed in steady state relative to the initial gain is characteristic of phased-array antennas and is commonly referred to as “projected aperture loss” due to scanning. This term derives from the fact that for large arrays this loss is quite accurately approximated by the cosine of the beam-steering angle from normal as if the effective aperture of the array is reduced by projection in the direction of the beam peak.

Finally, Fig. 4-4 shows the behavior of the far-zone beam as a sequence of step beam-steering detunings is applied.

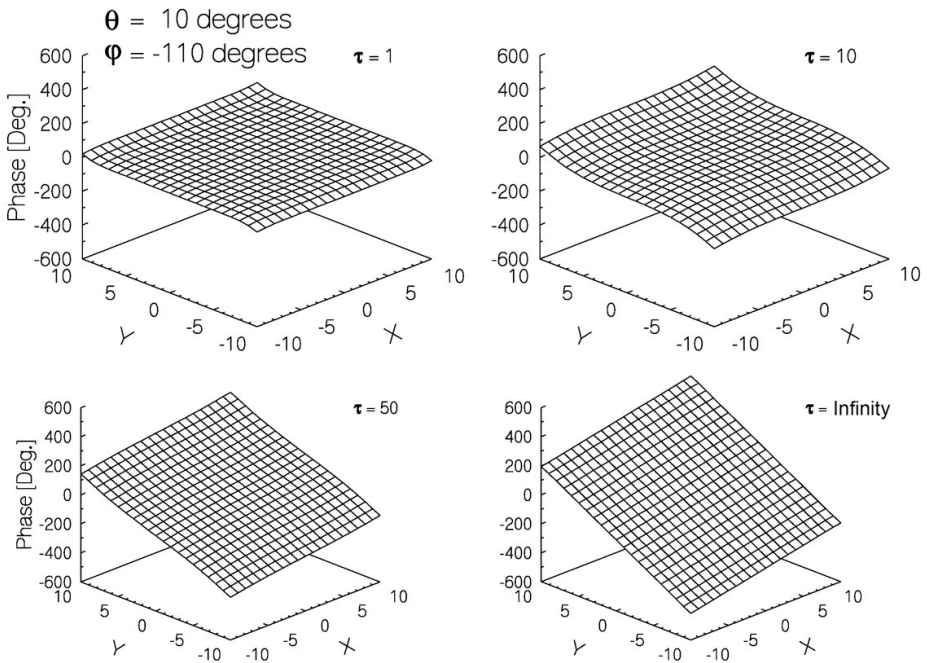


Fig. 4-1. Aperture phase distributions versus time in a two-dimensional array (edge oscillators detuned for beam-steering). (Reprinted from [42] with permission, ©2001 IEEE.)

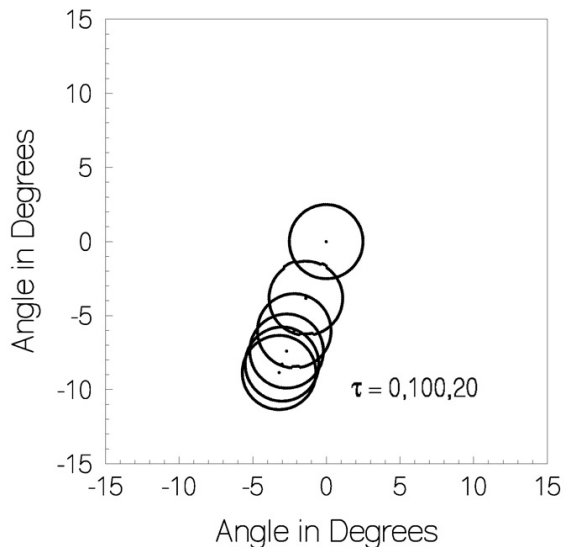


Fig. 4-2. Beam trajectory detuning during the beam-steering transient. (Reprinted from [42] with permission, ©2001 IEEE.)

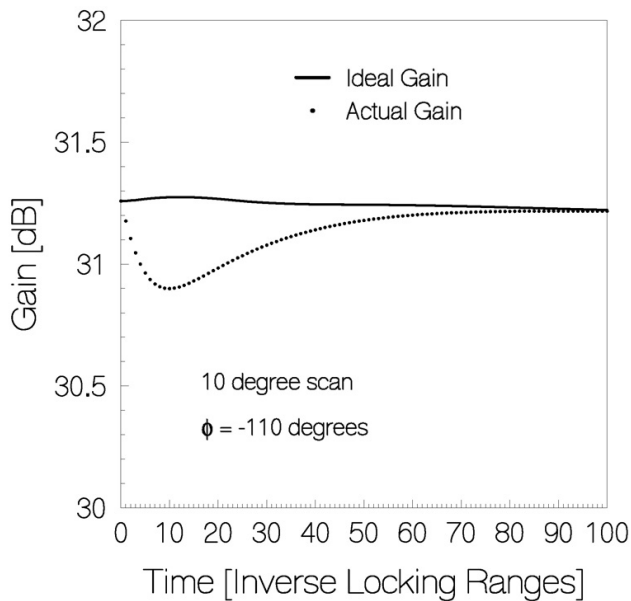


Fig. 4-3. Peak gain dynamics during the beam-steering transient. (Reprinted from [42] with permission, ©2001 IEEE.)

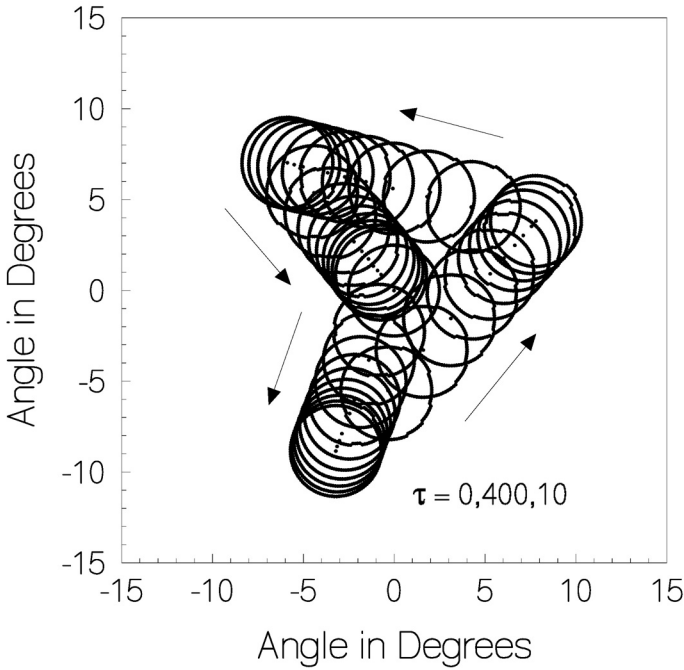


Fig. 4-4. Sequential beam-steering. (Reprinted from [42] with permission, ©2001 IEEE.)

4.2 Cartesian Coupling in the Continuum Model with External Injection

If beam-steering of a planar array is to be accomplished through external injection as proposed by Stephan [1], the continuum model is based on the two dimensional generalization of equation Eq. **Error! Reference source not found.**; that is,

$$\frac{\partial^2 \varphi}{\partial x^2} + \frac{\partial^2 \varphi}{\partial y^2} - V(x, y)\varphi - \frac{d\varphi}{d\tau} = -\Delta\Omega_{tune}(x, y, \tau) - V(x, y)\varphi_{inj}(x, y, \tau) \tag{4.2-1}$$

Now, because none of the oscillators are to be detuned, $\Delta\Omega_{tune} = 0$. Following Stephan [1], the perimeter oscillators are to be injection locked to external signals that are phase shifted with respect to one another to steer the beam. Thus, we choose the form,

$$V(x, y) = CP(x) + CQ(y) \tag{4.2-2}$$

where

$$C = \frac{\Delta\omega_{inj}}{\Delta\omega_{lock}} \quad (4.2-3)$$

and

$$\begin{aligned} CP(x) &= C_{x1}\delta(x-x'_1) + C_{x2}\delta(x-x'_2) \\ CQ(y) &= C_{y1}\delta(y-y'_1) + C_{y2}\delta(y-y'_2) \end{aligned} \quad (4.2-4)$$

so that Eq. (4.2-1) becomes,

$$\begin{aligned} \frac{\partial^2 \varphi}{\partial x^2} + \frac{\partial^2 \varphi}{\partial y^2} - CP(x)\varphi - CQ(y)\varphi - \frac{d\varphi}{d\tau} = \\ -CP(x)\varphi_{inj,x}(x, y, \tau) - CQ(y)\varphi_{inj,y}(x, y, \tau) \end{aligned} \quad (4.2-5)$$

where for notational convenience, we have separated the injection phases associated with the $P(x)$ and $Q(x)$ distributions of injection signals into the two functions, $\varphi_{inj,x}$ and $\varphi_{inj,y}$. Laplace transformation gives,

$$\begin{aligned} \frac{\partial^2 \tilde{\varphi}}{\partial x^2} + \frac{\partial^2 \tilde{\varphi}}{\partial y^2} - CP(x)\tilde{\varphi} - CQ(y)\tilde{\varphi} - s\tilde{\varphi} = \\ -CP(x)\tilde{\varphi}_{inj,x}(x, y, s) - CQ(y)\tilde{\varphi}_{inj,y}(x, y, s) \end{aligned} \quad (4.2-6)$$

Following [43], we now determine the eigenfunctions of the differential operator,

$$\frac{\partial^2}{\partial x^2} + \frac{\partial^2}{\partial y^2} - CP(x) - CQ(y) \quad (4.2-7)$$

subject to the Neumann boundary conditions at the array edges. Let the eigenfunctions be products of an x dependence and a y dependence; that is, $X(x, s_x)Y(y, s_y)$ so that by separation of variables we have,

$$\begin{aligned} X'' - CPX - s_x X &= 0 \\ Y'' - CQY - s_y Y &= 0 \end{aligned} \quad (4.2-8)$$

where the double primes indicate the second spatial derivative. Using Eq. (4.2-4), we obtain,

$$\begin{aligned} X'' - \Omega_{x1}\delta(x - x'_1)X - \Omega_{x2}\delta(x - x'_2)X - s_x X &= 0 \\ Y'' - \Omega_{y1}\delta(y - y'_1)Y - \Omega_{y2}\delta(y - y'_2)Y - s_y Y &= 0 \end{aligned} \quad (4.2-9)$$

First, consider the x dependent part. As in [43] the x region is divided into three parts, and a solution is postulated in each of these ranges of x . That is,

$$\begin{aligned} X &= A_1 \cosh \left[\sqrt{s_x} \left(a + \frac{1}{2} + x \right) \right] \cosh \left[\sqrt{s_x} \left(a + \frac{1}{2} - x'_1 \right) \right] \\ &+ A_2 \cosh \left[\sqrt{s_x} \left(a + \frac{1}{2} + x \right) \right] \cosh \left[\sqrt{s_x} \left(a + \frac{1}{2} - x'_2 \right) \right] \end{aligned} \quad (4.2-10)$$

$$\text{for } -a - \frac{1}{2} \leq x \leq x'_1$$

$$\begin{aligned} X &= A_1 \cosh \left[\sqrt{s_x} \left(a + \frac{1}{2} - x \right) \right] \cosh \left[\sqrt{s_x} \left(a + \frac{1}{2} + x'_1 \right) \right] \\ &+ A_2 \cosh \left[\sqrt{s_x} \left(a + \frac{1}{2} + x \right) \right] \cosh \left[\sqrt{s_x} \left(a + \frac{1}{2} - x'_2 \right) \right] \end{aligned} \quad (4.2-11)$$

$$\text{for } x'_2 \leq x \leq x'_1$$

$$\begin{aligned} X &= A_1 \cosh \left[\sqrt{s_x} \left(a + \frac{1}{2} - x \right) \right] \cosh \left[\sqrt{s_x} \left(a + \frac{1}{2} + x'_1 \right) \right] \\ &+ A_2 \cosh \left[\sqrt{s_x} \left(a + \frac{1}{2} - x \right) \right] \cosh \left[\sqrt{s_x} \left(a + \frac{1}{2} + x'_2 \right) \right] \end{aligned} \quad (4.2-12)$$

$$\text{for } x'_2 \leq x \leq a + \frac{1}{2}$$

This postulated solution satisfies the Neumann conditions at the array edges. The constants, A_1 and A_2 and the eigenvalues s_x , are determined by imposing the slope discontinuities across the injection points, x'_1 and x'_2 . That is,

$$\begin{aligned} X' \Big|_{x_1'}^{x_1'^+} &= C_{x1} X(x_1') \\ X' \Big|_{x_2'}^{x_2'^+} &= C_{x2} X(x_2') \end{aligned} \quad (4.2-13)$$

These conditions lead to two homogeneous linear equations for A_1 and A_2 which may be written in the form,

$$\begin{bmatrix} M_{11} & M_{12} \\ M_{21} & M_{22} \end{bmatrix} \begin{bmatrix} A_1 \\ A_2 \end{bmatrix} = \begin{bmatrix} 0 \\ 0 \end{bmatrix} \quad (4.2-14)$$

in which,

$$\begin{aligned} M_{11} &= \sqrt{s_x} \sinh \left[\sqrt{s_x} (2a+1) \right] \\ &+ C_{x1} \cosh \left[\sqrt{s_x} \left(a + \frac{1}{2} + x_1' \right) \right] \cosh \left[\sqrt{s_x} \left(a + \frac{1}{2} - x_1' \right) \right] \end{aligned} \quad (4.2-15)$$

$$M_{12} = C_{x1} \cosh \left[\sqrt{s_x} \left(a + \frac{1}{2} + x_1' \right) \right] \cosh \left[\sqrt{s_x} \left(a + \frac{1}{2} - x_2' \right) \right] \quad (4.2-16)$$

$$M_{21} = C_{x2} \cosh \left[\sqrt{s_x} \left(a + \frac{1}{2} + x_1' \right) \right] \cosh \left[\sqrt{s_x} \left(a + \frac{1}{2} - x_2' \right) \right] \quad (4.2-17)$$

$$\begin{aligned} M_{22} &= \sqrt{s_x} \sinh \left[\sqrt{s_x} (2a+1) \right] \\ &+ C_{x2} \cosh \left[\sqrt{s_x} \left(a + \frac{1}{2} + x_2' \right) \right] \cosh \left[\sqrt{s_x} \left(a + \frac{1}{2} - x_2' \right) \right] \end{aligned} \quad (4.2-18)$$

Setting the determinant of the two-by-two matrix in Eq. (4.2-14) equal to zero to permit a nontrivial solution for the A 's provides a transcendental equation for the eigenvalues, s_x . The eigenvalues all lie on the negative real axis of the s plane and can thus be easily computed numerically by any one-dimensional root finding method, such as the Newton-Raphson method. [46] For each value of s_x for which the determinant is zero, s_m , we have either that,

$$\begin{aligned} A_1 &= M_{12} \\ A_2 &= -M_{22} \end{aligned} \quad (4.2-19)$$

or that,

$$\begin{aligned} A_1 &= -M_{11} \\ A_2 &= M_{21} \end{aligned} \tag{4.2-20}$$

These two possible solutions are, in fact, the same to within a multiplicative constant but this constant has no effect once the eigenfunctions are normalized. Thus, either Eq. (4.2-19) or (4.2-20) may be used and the ultimate result will be the same. Normalization of the eigenfunctions is, of course, accomplished by integrating their square over the range of x ; that is, from $-(2a + 1)/2$ to $(2a + 1)/2$. This integration can be carried out giving a rather complicated but nevertheless closed-form result for the eigenfunction, $X(x, s_m)$.

Proceeding in the same manner one may obtain a corresponding closed form expression for $Y(y, s_n)$ and the Green's function, \tilde{g} , that satisfies,

$$\begin{aligned} \frac{\partial^2 \tilde{g}}{\partial x^2} + \frac{\partial^2 \tilde{g}}{\partial y^2} - [C_{x1}\delta(x - x'_1) + C_{x2}\delta(x - x'_2)] \tilde{g} \\ - [C_{y1}\delta(y - y'_1) + C_{y2}\delta(y - y'_2)] \tilde{g} \tag{4.2-21} \\ - s\tilde{g} = -\frac{1}{s} \delta(x - x')\delta(y - y') \end{aligned}$$

may then be expressed in the form,

$$\tilde{g} = \sum_{n=0}^{\infty} \sum_{m=0}^{\infty} \frac{X(x', s_m)Y(y', s_n)X(x, s_m)Y(y, s_n)}{s(s - s_m + s_n)} \tag{4.2-22}$$

Now the solution to Eq. (4.2-6) is,

$$\begin{aligned} \tilde{\varphi}(x, y, s) = -\int_{-b-\frac{1}{2}}^{b+\frac{1}{2}} \int_{-a-\frac{1}{2}}^{a+\frac{1}{2}} \tilde{g}(x', y', x, y, s) \\ [P(x')\tilde{\varphi}_{inj,x}(x', y', s) + Q(y')\tilde{\varphi}_{inj,y}(x', y', s)] dx' dy' \end{aligned} \tag{4.2-23}$$

where P and Q are given by Eq. (4.2-4). The presence of the Dirac delta functions in Eq. (4.2-4) facilitates the integration. Let,

$$\tilde{\varphi}_{inj}(x, y, s) = \frac{1}{s} \tag{4.2-24}$$

so that the injection phase time dependence is a step function. The inverse Laplace transform is then computable as a sum of the residues, $R_{mn}(x,y)$, at the poles in Eq. (4.2-22) where $s = s_m + s_n$. Thus, the solution takes the form,

$$\varphi(x, y, \tau) = \sum_{n=0}^{\infty} \sum_{m=0}^{\infty} R_{mn}(x, y) \left[1 - e^{(s_m + s_n)\tau} \right] u(\tau) \quad (4.2-25)$$

Note that while there is a pole at $s = 0$, its residue is zero so Eq. (4.2-22) does not have a double pole at $s = 0$ and the inverse Laplace transform does not have a term linear in time. Therefore, there is no frequency shift as there was in the case of perimeter detuning. Because there is no detuning, the ensemble frequency of the array does not change. The injection frequencies are all equal to this ensemble frequency so all oscillation remains at this same frequency. Were the injection frequency different from the ensemble frequency, the steady-state oscillation frequency would be equal to the injection frequency and a term linear in time would appear in the solution.

The desired steady-state solution (for infinite time) is a planar phase distribution. We can determine the injection phases needed to produce that steady state directly from Eq. (4.2-5). Let us use uniform-strength injection signals so that,

$$C_{x2} = C_{x1} = C_{y2} = C_{y1} = C_{inj} \quad (4.2-26)$$

At infinite time, Eq. (4.2-5) becomes,

$$\begin{aligned} \frac{\partial^2 \varphi_{ss}}{\partial x^2} + \frac{\partial^2 \varphi_{ss}}{\partial y^2} = & \left[C_{x1} \delta(x - x'_1) + C_{x2} \delta(x - x'_2) \right] (\varphi_{inj} - \varphi_{ss}) \\ & + \left[C_{y1} \delta(y - y'_1) + C_{y2} \delta(y - y'_2) \right] (\varphi_{inj} - \varphi_{ss}) \end{aligned} \quad (4.2-27)$$

The right side of this equation is zero except on the extended perimeter of a rectangle defined by,

$$(x - x'_1)(x - x'_2)(y - y'_1)(y - y'_2) = 0 \quad (4.2-28)$$

Thus, the left side must also be zero except on these four lines. The solution we seek is linear in x and y , and will have slope discontinuities on the rectangle defined by Eq. (4.2-28). The slope of the phase surface will be set by the desired beam direction as in Eq. (4.1-11). Thus,

$$\varphi_{ss}(x, y) = \frac{\Omega_x}{2} (|x - x'_1| - |x - x'_2|) + \frac{\Omega_y}{2} (|y - y'_1| - |y - y'_2|) \quad (4.2-29)$$

Substituting Eq. (4.2-29) into Eq. (4.2-27), we obtain,

$$\begin{aligned} & \varphi_{inj,x}(x, y) [C_{x1} \delta(x - x'_1) + C_{x2} \delta(x - x'_2)] \\ & + \varphi_{inj,y}(x, y) [C_{y1} \delta(y - y'_1) + C_{y2} \delta(y - y'_2)] = \\ & \left[-\Omega_x - C_{x1} \frac{\Omega_x}{2} |x'_2 - x'_1| + C_{x1} \frac{\Omega_y}{2} (|y - y'_1| - |y - y'_2|) \right] \delta(x - x'_1) + \\ & \left[\Omega_x + C_{x2} \frac{\Omega_x}{2} |x'_2 - x'_1| + C_{x2} \frac{\Omega_y}{2} (|y - y'_1| - |y - y'_2|) \right] \delta(x - x'_2) + \quad (4.2-30) \\ & \left[-\Omega_y - C_{y1} \frac{\Omega_y}{2} |y'_2 - y'_1| + C_{y1} \frac{\Omega_x}{2} (|x - x'_1| - |x - x'_2|) \right] \delta(y - y'_1) + \\ & \left[\Omega_y + C_{y2} \frac{\Omega_y}{2} |y'_2 - y'_1| + C_{y2} \frac{\Omega_x}{2} (|x - x'_1| - |x - x'_2|) \right] \delta(y - y'_2) \end{aligned}$$

so that the required injection phases may be written,

$$\begin{aligned} \varphi_{inj,x}(x, y) = & \frac{\Omega_x}{2} \left[(|x - x'_1| - |x - x'_2|) \right. \\ & \left. + \frac{2}{C_{x1}} \frac{(x - x'_2)}{|x'_1 - x'_2|} + \frac{2}{C_{x2}} \frac{(x - x'_1)}{|x'_1 - x'_2|} \right] \quad (4.2-31) \end{aligned}$$

$$\begin{aligned} \varphi_{inj,y}(x, y) = & \frac{\Omega_y}{2} \left[(|y - y'_1| - |y - y'_2|) \right. \\ & \left. + \frac{2}{C_{y1}} \frac{(y - y'_2)}{|y'_1 - y'_2|} + \frac{2}{C_{y2}} \frac{(y - y'_1)}{|y'_1 - y'_2|} \right] \quad (4.2-32) \end{aligned}$$

For these injection phases, at late times, Eq. (4.2-25) is very slowly converging. However, we may remedy this as follows. If the Fourier series for the steady-state solution Eq. (4.2-29) is subtracted from the solution Eq. (4.2-25), the resulting series converges rapidly for late times. Then to obtain the complete late time solution one merely adds the steady-state solution Eq. (4.2-29) to this rapidly converging series. This solution conveniently complements the form

given by Eq. (4.2-25) that converges rapidly for early times. (Convergence acceleration of this sort may also be applied in steering via detuning and in the one-dimensional cases treated in Chapter 3 if desired.)

If C_{inj} is large (strong injection), the last two terms in each of Eqs. (4.2-31) and (4.2-32) are negligible, and the injection phase equals the desired steady-state phase at the injection points as in the one-dimensional case. This strong injection assumption was implicit in the analyses presented in Refs. [39] and [43] because the small terms were neglected in accelerating the series, but this fact was not explicitly noted.

As an example, the solution given by Eq. (4.2-25) was computed for a 21-by-21 element array with injection signals of strength parameter C equal to 0.7 on the perimeter phased to steer the beam 10 deg from normal at -110 deg of azimuth. This requires that we apply the phase shift gradually as discussed in Section 3.4. We choose to do this linearly over an interval of 50 inverse locking ranges, after which the injection phases become constant. The solution for linear-injection phase can be obtained from that for constant-injection phase by integration with respect to time or division by s in the Laplace domain. The phase distributions across the array at four instants of time are shown in Fig. 4-5. Figure 4-6 shows the corresponding trajectory of the beam peak and 3-dB contour during the beam-steering transient at intervals of 10 inverse locking ranges. Here again, as shown in Fig. 4-7, because of the phase aberration (deviation from planarity) across the aperture during the transient, the directivity of the antenna decreases, but this loss is recovered in steady state when the phase distribution again becomes planar. The so-called “projected aperture loss” discussed in Section 4.1 is also clearly visible. Finally, Fig. 4-8 shows the result of applying a sequence of injection phases resulting in sequential beam-steering to several angles.

4.3 Non-Cartesian Coupling Topologies

The planar arrays presented so far have made use of a Cartesian coupling topology in which oscillators on a Cartesian lattice were coupled to four nearest neighbors. However, this is by no means the only coupling topology leading to planar arrays that admit beam-steering. In this section we treat, via the continuum formulation, two other possible topologies, triangular (Fig. 4-9) and hexagonal (Fig. 4-10).

In the triangular case, shown in Fig. 4-9, the unit cells are hexagons and each interior oscillator is coupled to six nearest neighbors. [44] The oscillators are identified with pairs of integer values of the coordinates p and q ranging from 1 to N .

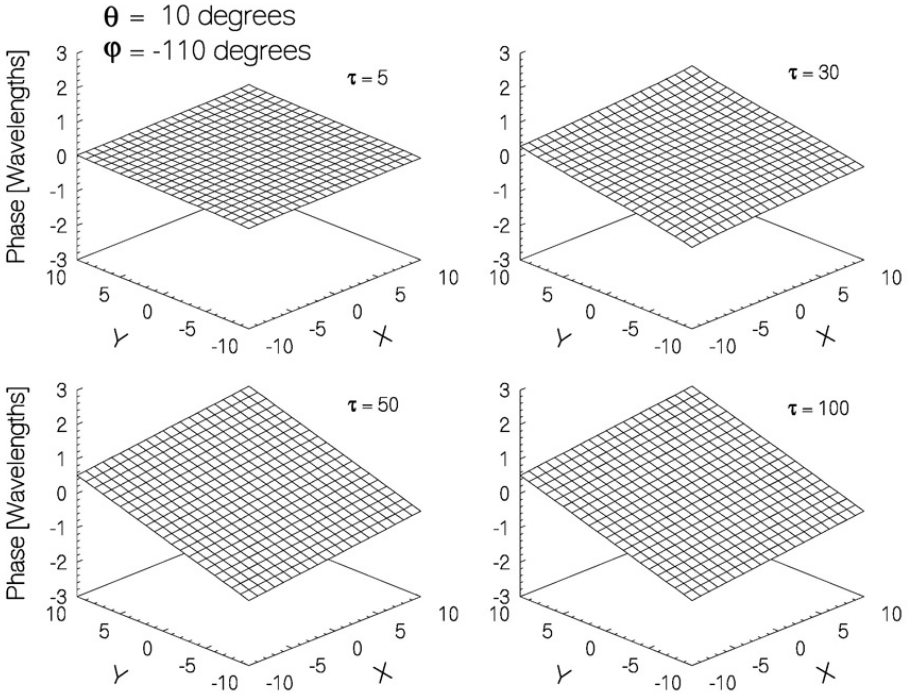


Fig. 4-5. Aperture phase distributions versus time (edge oscillators injection locked for beam-steering). (Reprinted from [43] with permission, ©2001 IEEE.)

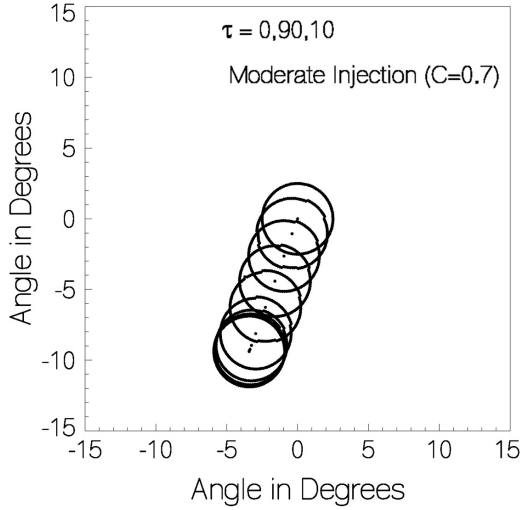


Fig. 4-6. Beam trajectory during the beam-steering transient. (Reprinted from [43] with permission, ©2001 IEEE.)

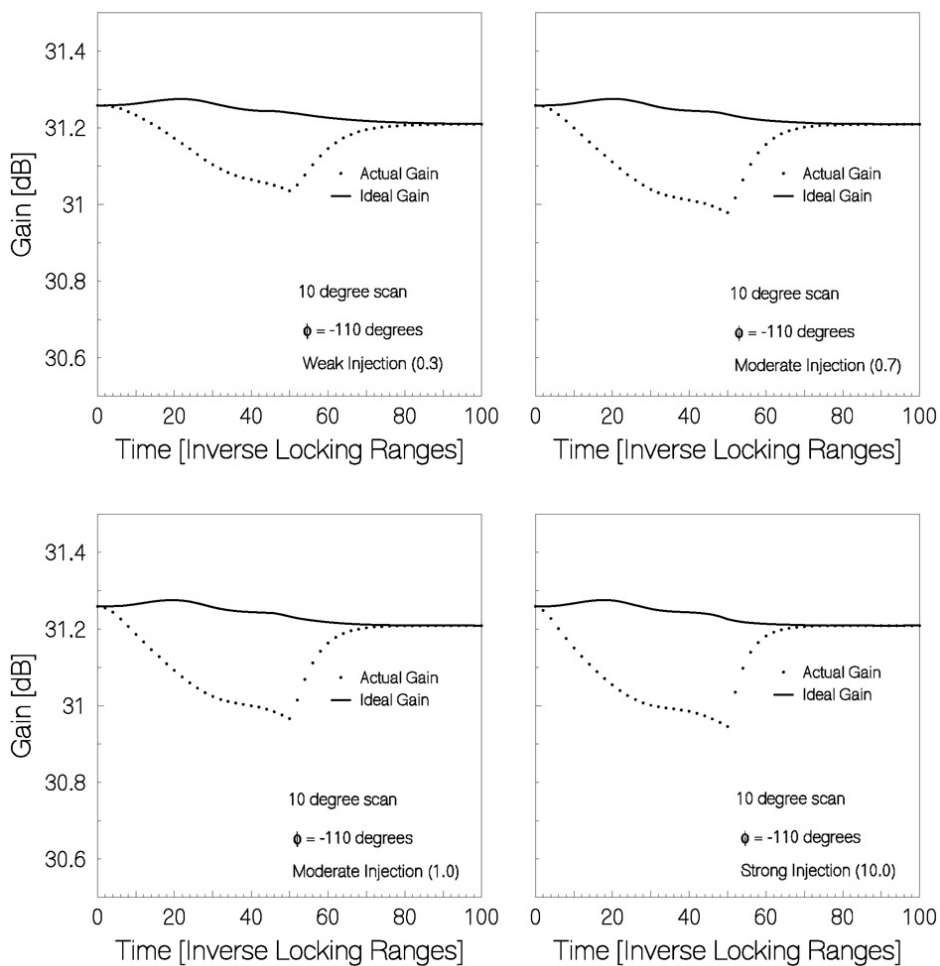


Fig. 4-7. Peak gain dynamics during the beam-steering transient for various injection strengths. (Reprinted from [43] with permission, ©2001 IEEE.)

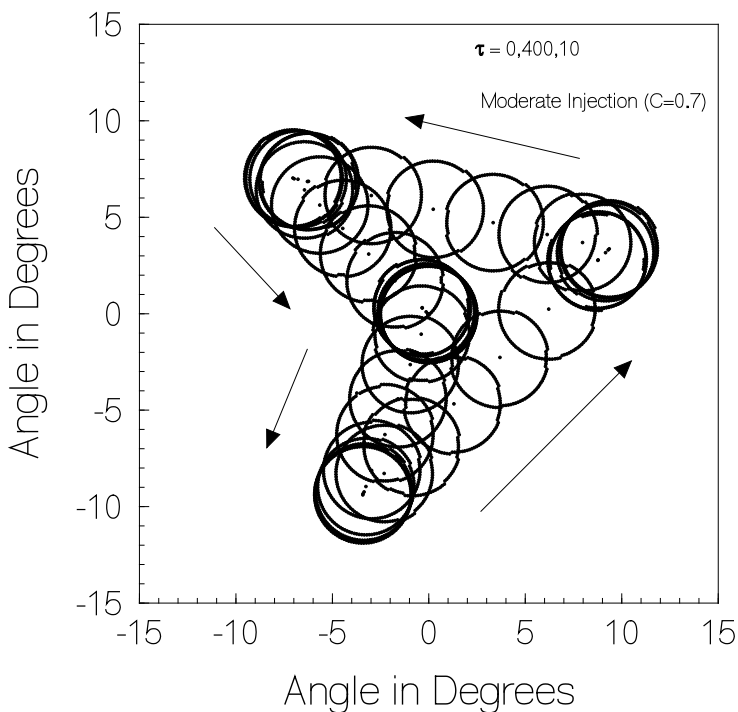


Fig. 4-8. Sequential beam-steering (τ varies from 0 to 400 in increments of 10). (Reprinted from [43] with permission, ©2001 IEEE.)

Using these coordinates, the discrete model yields the system of differential equations,

$$\begin{aligned}
 \frac{\partial \varphi_{pq}}{\partial t} &= \omega_{tune,pq} - \omega_{ref} \\
 -\Delta \omega_{lock} & \left[\sin(\varphi_{pq} - \varphi_{p-1,q}) + \sin(\varphi_{pq} - \varphi_{p+1,q}) \right. \\
 & \quad + \sin(\varphi_{pq} - \varphi_{p+1,q-1}) + \sin(\varphi_{pq} - \varphi_{p,q-1}) \\
 & \quad \left. + \sin(\varphi_{pq} - \varphi_{p,q+1}) + \sin(\varphi_{pq} - \varphi_{p-1,q+1}) \right]
 \end{aligned} \tag{4.3-1}$$

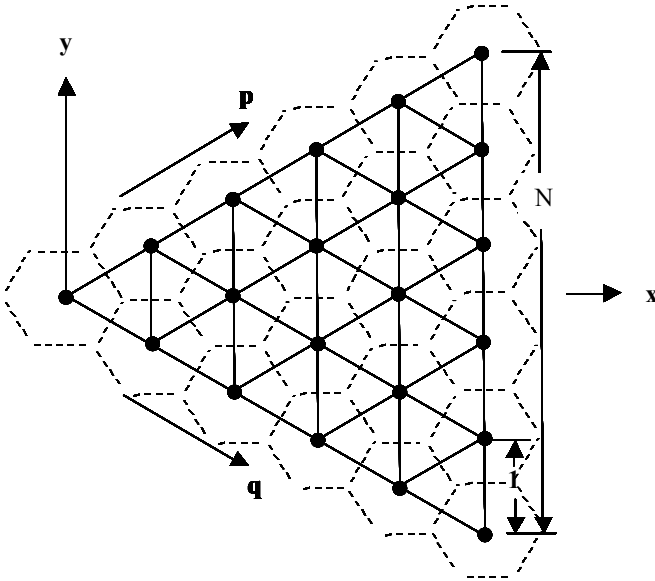


Fig. 4-9. Oscillators coupled on an equilateral triangular lattice. (Reprinted with permission from [44], ©2004 IEEE.)

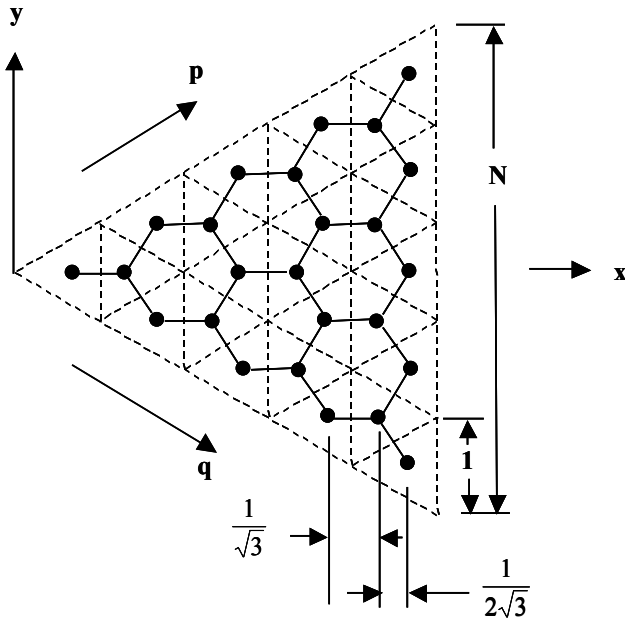


Fig. 4-10. Oscillators coupled on a hexagonal lattice. (Reprinted with permission from [44], ©2004 IEEE.)

where we have assumed that the coupling phases are multiples of 2π . We remark that this system of nonlinear equations can be solved numerically to yield the full nonlinear solution for the dynamic behavior of the phase distribution. However, as mentioned earlier, the analytic solution of the linearized formulation provides more insight. Linearizing and expanding in Taylor series to second order leads to,

$$2\left(\frac{\partial^2 \varphi}{\partial p^2} + \frac{\partial^2 \varphi}{\partial p \partial q} + \frac{\partial^2 \varphi}{\partial q^2}\right) - \frac{\partial \varphi}{\partial \tau} = -\Delta \Omega_{tune}(p, q) \quad (4.3-2)$$

where, as before, $\tau = \Delta \omega_{lock} t$ and $\Delta \Omega_{tune} = (\omega_{tune} - \omega_{ref}) / \Delta \omega_{lock}$. Transforming to Cartesian coordinates, x and y , we arrive at,

$$\left(\frac{\partial^2 \varphi}{\partial x^2} + \frac{\partial^2 \varphi}{\partial y^2}\right) - \frac{\partial \varphi}{\partial T_{tri}} = -\frac{1}{\sqrt{3}} \Delta \Omega_{tune} \quad (4.3-3)$$

and $T_{tri} = (3/2)\tau$. This equation is very much like Eq. (4.1-2) for the Cartesian case except for the scaling of the time and the detuning.

In the hexagonal case, shown in Fig. 4-10, the unit cells are triangular and each interior oscillator is coupled to three nearest neighbors [44]. Following a procedure analogous to that presented above for the triangular case leads to,

$$\left(\frac{\partial^2 \varphi}{\partial x^2} + \frac{\partial^2 \varphi}{\partial y^2}\right) - \frac{\partial \varphi}{\partial T_{hex}} = -\sqrt{3} \Delta \Omega_{tune} \quad (4.3-4)$$

and $T_{hex} = \tau/4$. Again, this equation is very much like Eq. (4.1-2) for the Cartesian case except for the scaling of the time and the detuning.

Finite arrays using the triangular and hexagonal coupling schemes may be constructed with equilateral triangular boundaries, and the boundary conditions on the phase will again be of the Neumann type. Just as was the case for rectangular arrays, if the oscillators on the triangular boundary are detuned, the steady-state interior phases are governed by Laplace's equation, and planar distributions are an obtainable special case. The desired steady-state solution to produce a beam steered to spherical coordinate angles, (θ_0, φ_0) , is,

$$\varphi(x, y, \infty) = -\frac{2\pi d}{\lambda} \left[\left(x - \frac{N}{\sqrt{3}} \right) \sin \theta_0 \cos \varphi_0 + y \sin \theta_0 \sin \varphi_0 \right] \quad (4.3-5)$$

where d is the separation of the radiating elements in the y coordinate for fixed x , and λ is the wavelength. Substituting this desired steady-state phase distribution, Eq. (4.3-5), into the partial differential equations, Eqs. (4.3-3) and (4.3-4), gives the required detuning of the perimeter oscillators.

$$\begin{aligned}\Delta\Omega_{tune}|_{x=y\sqrt{3}} &= -\frac{2\pi d}{\alpha\lambda} \sin\theta_0 \cos\left(\varphi_0 - \frac{2\pi}{3}\right) \\ \Delta\Omega_{tune}|_{x=-y\sqrt{3}} &= -\frac{2\pi d}{\alpha\lambda} \sin\theta_0 \cos\left(\varphi_0 + \frac{2\pi}{3}\right) \\ \Delta\Omega_{tune}|_{x=A\sqrt{3}/2} &= -\frac{2\pi d}{\alpha\lambda} \sin\theta_0 \cos(\varphi_0)\end{aligned}\quad (4.3-6)$$

where A is the length of a side of the array, Nd , and α is $1/\sqrt{3}$ for the triangular coupling and $\sqrt{3}$ for hexagonal coupling. Note that the sum of these detunings is zero for all steering angles so that the ensemble frequency of the array is unchanged.

At this point we note for later reference that it is possible to obtain the needed tuning for a given planar steady-state phase distribution from the full nonlinear formulation Eq. (4.3-1). Inserting the desired phase Eq. (4.3-5) into Eq. (4.3-1) and evaluating on the boundary of the triangle we obtain,

$$\begin{aligned}\Delta\Omega_{tune}|_{x=y\sqrt{3}} &= \frac{1}{\sqrt{3}} \sin\left[\frac{2\pi d}{\alpha\lambda} \sin\theta_0 \cos\left(\varphi_0 + \frac{\pi}{6}\right)\right] \\ &\quad + \frac{1}{\sqrt{3}} \sin\left[\frac{2\pi d}{\alpha\lambda} \sin\theta_0 \cos\left(\varphi_0 + \frac{\pi}{2}\right)\right] \\ \Delta\Omega_{tune}|_{x=-y\sqrt{3}} &= \frac{1}{\sqrt{3}} \sin\left[\frac{2\pi d}{\alpha\lambda} \sin\theta_0 \cos\left(\varphi_0 - \frac{\pi}{6}\right)\right] \\ &\quad + \frac{1}{\sqrt{3}} \sin\left[\frac{2\pi d}{\alpha\lambda} \sin\theta_0 \cos\left(\varphi_0 - \frac{\pi}{2}\right)\right] \\ \Delta\Omega_{tune}|_{x=A\sqrt{3}/2} &= \frac{1}{\sqrt{3}} \sin\left[\frac{2\pi d}{\alpha\lambda} \sin\theta_0 \cos\left(\varphi_0 - \frac{5\pi}{6}\right)\right] \\ &\quad + \frac{1}{\sqrt{3}} \sin\left[\frac{2\pi d}{\alpha\lambda} \sin\theta_0 \cos\left(\varphi_0 + \frac{5\pi}{6}\right)\right]\end{aligned}\quad (4.3-7)$$

which reduces to Eq. (4.3-6) for small θ_0 ; that is, for small inter-oscillator phase differences when the linearization is accurate. Note that the sum of these detunings is exactly zero regardless of steering angle.

We propose that the solutions of the partial differential equations, Eq. (4.3-3) and Eq. (4.3-4), be obtained as series of the eigenfunctions of the differential operators subject to Neumann boundary conditions on the triangular boundary of the arrays. These eigenfunctions have been studied in the context of waveguides of triangular cross section and are thus well known. They are expressed as sums of three products of two of the trigonometric functions, sine and cosine. These eigenfunctions and their useful properties are summarized in the appendix of Ref. [44].

We wish to solve,

$$\left(\frac{\partial^2 \varphi}{\partial x^2} + \frac{\partial^2 \varphi}{\partial y^2} \right) - \frac{\partial \varphi}{\partial T} = -\alpha \Delta \Omega_{tune} \quad (4.3-8)$$

with the detuning function given by Eq. (4.3-6), and we will assume that the detuning is a step function in time. Laplace transformation of Eq. (4.3-8) gives,

$$\left(\frac{\partial^2 \tilde{\varphi}}{\partial x^2} + \frac{\partial^2 \tilde{\varphi}}{\partial y^2} \right) - s \tilde{\varphi} = -\alpha \Delta \tilde{\Omega}_{tune} = -\frac{\alpha}{s} \Delta \Omega_{tune}(x, y) \quad (4.3-9)$$

The solution will be of the form,

$$\varphi(x, y, \tau) = \sum_{mn} C_{mn} H_{mn}^{(i)}(x, y) \left(1 - e^{-\sigma_{mn} T} \right) u(T) \quad (4.3-10)$$

where the H functions are the normalized eigenfunctions on the triangle with the superscript denoting even or odd symmetry of the function in y . Thus, the unknown coefficients may be found from the desired steady-state phase distribution, Eq. (4.3-5), by setting T to infinity in Eq. (4.3-10) and setting the resulting sum equal to the steady-state solution. Then, the orthogonality of the eigenfunctions permits us to find the coefficients, C_{mn} . This procedure is completely equivalent to expressing the Green's function as a sum of the eigenfunctions and then integrating the product of the Green's function and the desired steady-state phase distribution as was done in the Cartesian case.

As was done in Ref. [44], we now provide a number of computed examples demonstrating the dynamic behavior obtained via the various formulations of the problem; that is, the nonlinear model, the linearized discrete model, and the continuum model for both the triangular and hexagonal coupling topologies.

We begin with triangular coupling with $N = 28$ resulting in a 435-oscillator array. We completely preclude the appearance of grating lobes in the visible region by selecting the radiating element spacing, d , to be $\lambda/\sqrt{3}$. We note, however, that, because the maximum permissible phase difference between coupled oscillators is 90 deg, the element spacing can be as large as $\lambda\sqrt{3}/2$ without the appearance of visible grating lobes. The array size, A , in the continuum model is taken to be $d\sqrt{(N+1)(N+2)}$ instead of Nd because that makes the array area equal to the sum of the unit cell areas, resulting in a more accurate directivity. Figure 4-11 shows the aperture phase distribution for four instants of time computed using the continuum model with perimeter detuning given by Eq. (4.3-6) and unit step temporal dependence and steady-state beam-pointing angles $(\theta_0, \varphi_0) = 10$ deg, 45 deg). Note the rather severe phase aberration at time equal to 10 inverse locking ranges. Figure 4-12 shows the directivity (gain in the absence of loss) computed by pattern integration as a function of time during the beam-steering transient. The solid curve is the result of planar phase distribution, and “projected aperture loss” is again evident. In the left plot, the continuum result is compared with the full nonlinear solution obtained numerically, and in the right plot the numerical solution of the linearized discrete model is compared with the nonlinear solution. Note that the dip in gain at about 10 inverse locking ranges correlates with the severe aberration at that time in Fig. 4-11. The nonlinear solution used Eq. (4.3-7) while the linear ones used Eq. (4.3-6) as detuning. Because the angle from normal is only 10 deg, the error in the linear approximation of the sine functions is less than 6.5 percent, and the linearized and continuum results agree well with the full nonlinear result taken to be the correct behavior. Figure 4-13 shows the trajectory of the beam peak and 3-dB contour during the beam-steering transient as computed via the three formulations, and, as should be expected for this small steering angle, they agree very well.

Now, if the final beam angle is increased from 10 deg to 25 deg, the error in the linear approximation of the sine function is almost 49 percent, and the discrepancy between the linear and nonlinear results in Fig. 4-14 show the impact of this in that the gain error at the dip is about 2 dB, and the curves are slightly different in shape. However, there is still qualitative agreement between the linear and nonlinear results.

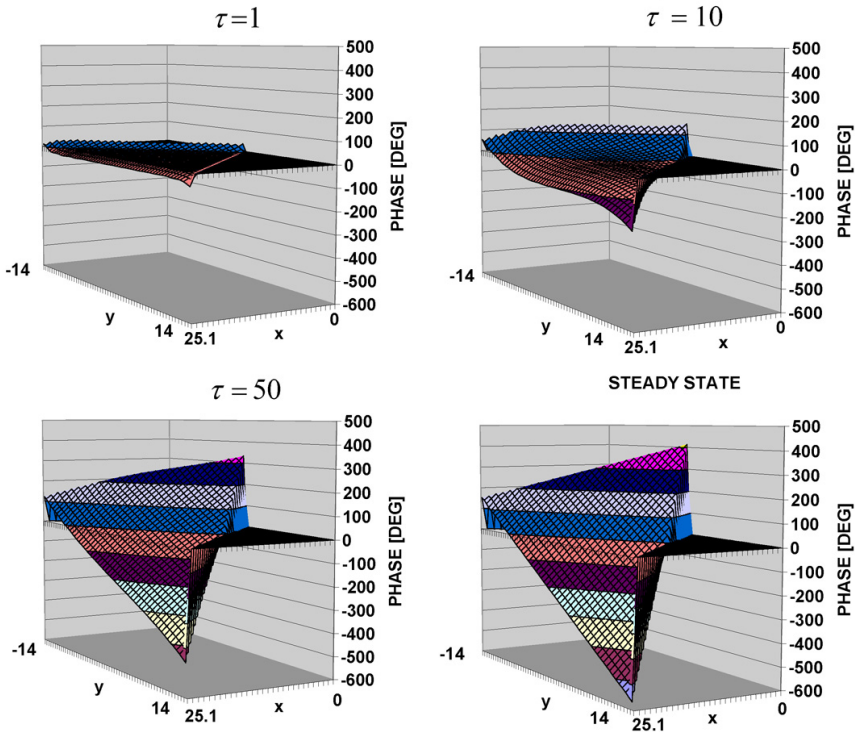


Fig. 4-11. Aperture phase distributions for triangular coupling with $(\theta_0, \varphi_0) = (10 \text{ deg}, 45 \text{ deg})$ for τ values of 1, 10, and 50, plus steady state. (Reprinted with permission from [44], ©2004 IEEE.)

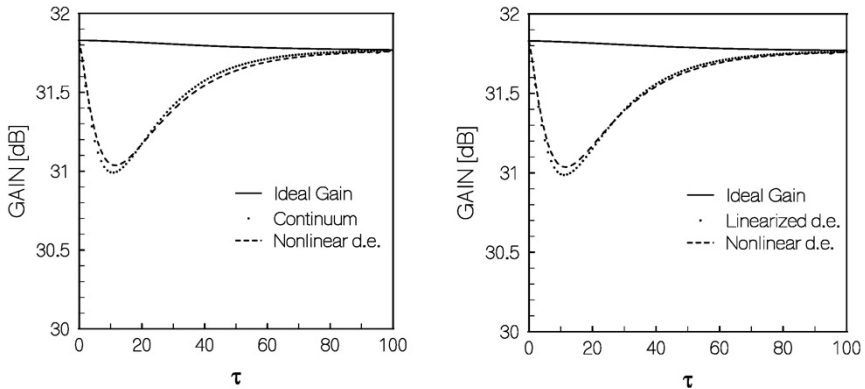


Fig. 4-12. Gain dynamics of gain plotted against percentage of τ for triangular coupling with $(\theta_0, \varphi_0) = (10 \text{ deg}, 45 \text{ deg})$. (Reprinted with permission from [44], ©2004 IEEE.)

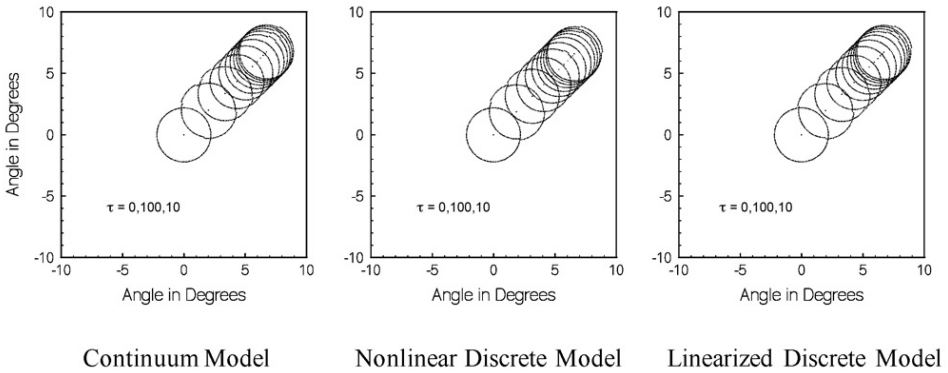


Fig. 4-13. Beam dynamics for triangular coupling with $(\theta_0, \phi_0) = (10 \text{ deg}, 45 \text{ deg})$. (Reprinted with permission from [44], ©2004 IEEE.)

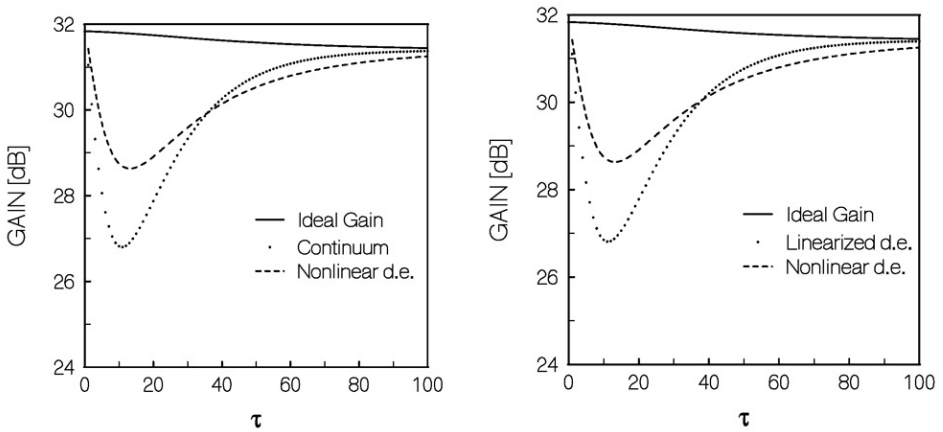


Fig. 4-14. Gain dynamics for triangular coupling with $(\theta_0, \phi_0) = (25 \text{ deg}, 45 \text{ deg})$. (Reprinted with permission from [44], ©2004 IEEE.)

Figure 4-15 shows the trajectory of the beam peak and the 3-dB contour during the beam-steering transient as computed using the three formulations and the agreement among them is good even though the accuracy of the linearization is questionable.

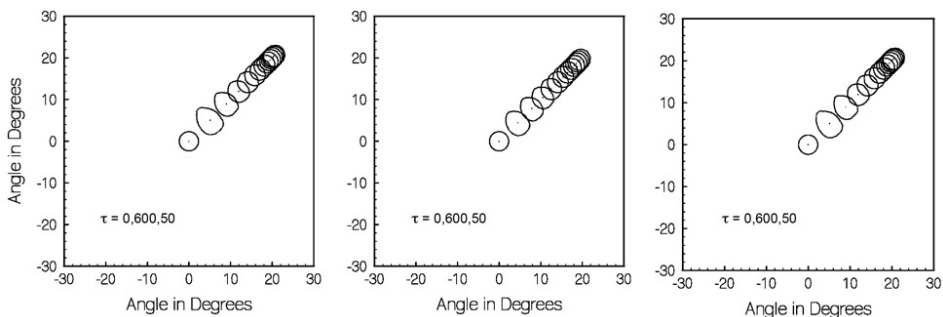


Fig. 4-15. Beam dynamics for triangular coupling with $(\theta_0, \varphi_0) = (25 \text{ deg}, 45 \text{ deg})$. (τ varies from 0 to 600 in increments of 50.) (Reprinted with permission from [44], ©2004 IEEE.)

Consider now a hexagonally coupled array in which we again choose d to be $\lambda/\sqrt{3}$. If we choose N to be 28, this hexagonally coupled array will have 784 oscillators. This makes the distance between the corner elements a bit less than in the triangular case for $N = 28$. Choosing the array size, A , to be Nd here makes the array area equal to the sum of the unit cell areas as was done for the triangular coupling example. Assuming that the radiating elements are arranged as in Fig. 4-10, the separation between periodic lines of elements will be $\lambda/2$, and there will be no grating lobes in the visible region. Here again, however, the spacing d can be as large as $\lambda\sqrt{3}/2$ and still not produce grating lobes because the phase differences must be less than 90 deg to maintain lock.

Figure 4-16 shows the aperture phase distribution at a sequence of times for steady-state beam-steering angles of $(\theta_0, \varphi_0) = (20 \text{ deg}, 45 \text{ deg})$. The behavior is very similar to that observed with triangular coupling except for the time scale of the response, which is considerably slower for the hexagonal coupling. Of course, one must remember that this array has many more oscillators than the triangular one. The temporal behavior of the gain of this array is shown in Fig. 4-17 as computed using the full nonlinear model, the linearized model, and the continuum model. Because for this steady-state beam-steering angle, the error in the linear approximation to the sine function is only about 9 percent, these results agree quite well. The dip in the gain at about 60 inverse locking ranges is consistent with the significant phase aberration seen at that time in Fig. 4-16. Finally the trajectories of the beam peak and 3-dB contour as computed using the three formulations are shown in Fig. 4-18 for a steady-state beam position 20 deg from normal to the array. If this angle is increased to 30 deg, the approximation error increases to about 20 percent, and Fig. 4-19

shows the impact of this in terms of the discrepancies between the full nonlinear result taken to be correct and those of the two linearized theories. Finally Fig. 4-20 shows the corresponding beam trajectories.

As pointed out in [44], it might seem appropriate to correct the detuning needed for a given set of steady-state beam-steering angles as was done for triangular coupling in the manner of (4.3-7) but this is not very effective for reasons that will become clear as we discuss the true steady-state phase distribution for a hexagonally coupled array. [45] For one thing, there is a tendency to choose detunings that do not sum to zero thus producing quadratic phase distributions instead of planar ones. One may artificially impose a zero sum but the proper choice of detuning still lacks a firm theoretical basis.

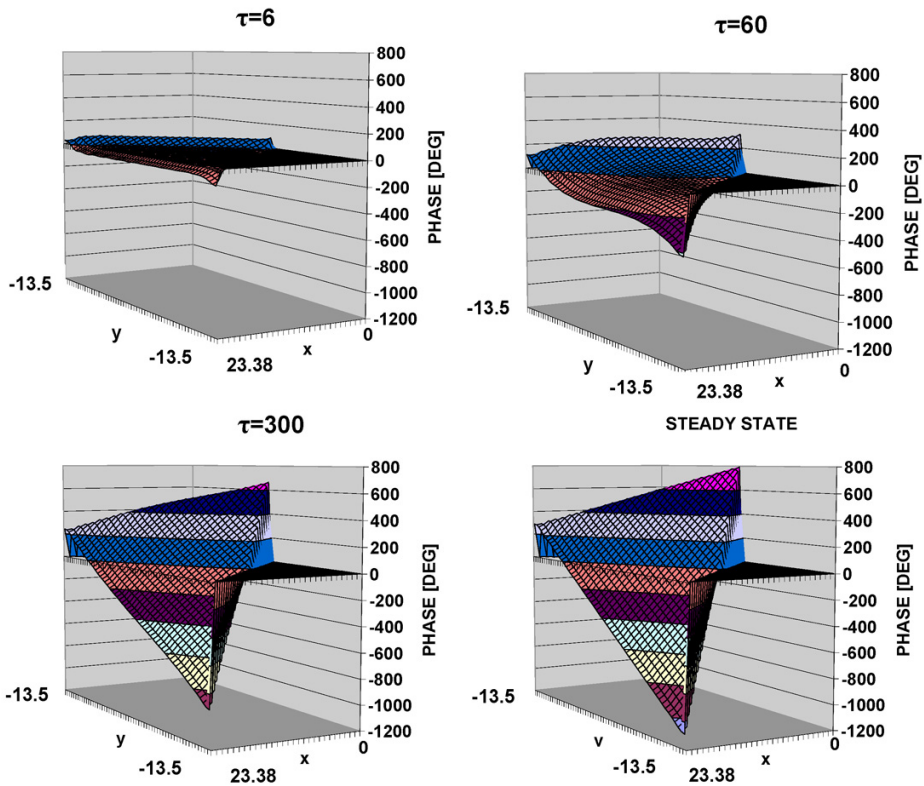


Fig. 4-16. Aperture phase for hexagonal coupling with $(\theta_0, \varphi_0) = (20 \text{ deg}, 45 \text{ deg})$.
(Reprinted with permission from [44], ©2004 IEEE.)

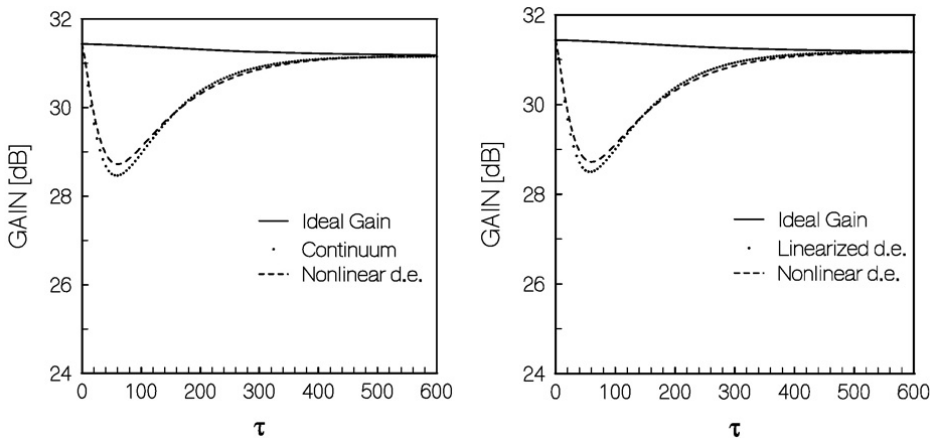


Fig. 4-17. Gain dynamics for hexagonal coupling with $(\theta_0, \phi_0) = (20 \text{ deg}, 45 \text{ deg})$ (Reprinted with permission from [44], ©2004 IEEE.)

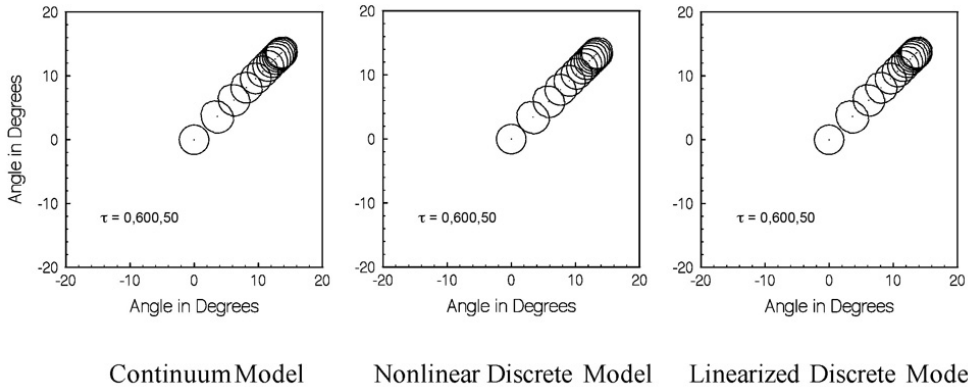


Fig. 4-18. Beam dynamics for hexagonal coupling with $(\theta_0, \phi_0) = (20 \text{ deg}, 45 \text{ deg})$ (τ varies from 0 to 600 in increments of 50). (Reprinted with permission from [44], ©2004 IEEE.)

To obtain the results shown in Figs. 4-19 and 4-20, a correction factor was applied to the three detunings of Eq. (4.3-6). The factor was derived at an azimuth angle of 30 deg because, as will be seen, it is only at 30 deg plus integral multiples of 60 deg that planar phase distributions are rigorous steady-state solutions for the phase distribution. For reference, this correction factor as given in Ref. [44] is,

$$Correction\ Factor = \frac{\sin\left[\frac{2\pi d}{\alpha\lambda}\sin\theta_0\cos\left(\frac{\pi}{6}\right)\right]}{\frac{2\pi d}{\alpha\lambda}\sin\theta_0\cos\left(\frac{\pi}{6}\right)} \quad (4.3-11)$$

and this factor is multiplied by each of the edge detunings in Eq. (4.3-6), thus preserving the zero sum.

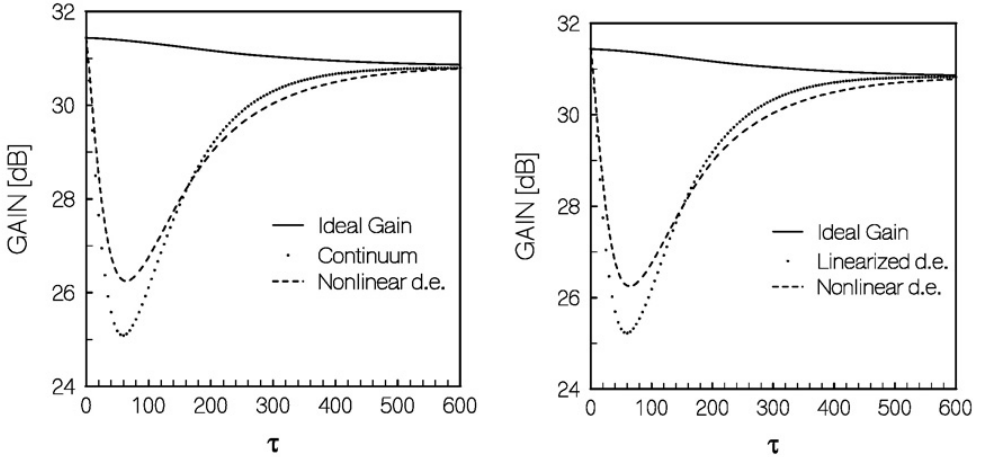


Fig. 4-19. Gain dynamics for hexagonal coupling with $(\theta_0, \varphi_0) = (30\text{ deg}, 45\text{ deg})$ (Reprinted with permission from [44], ©2004 IEEE.)

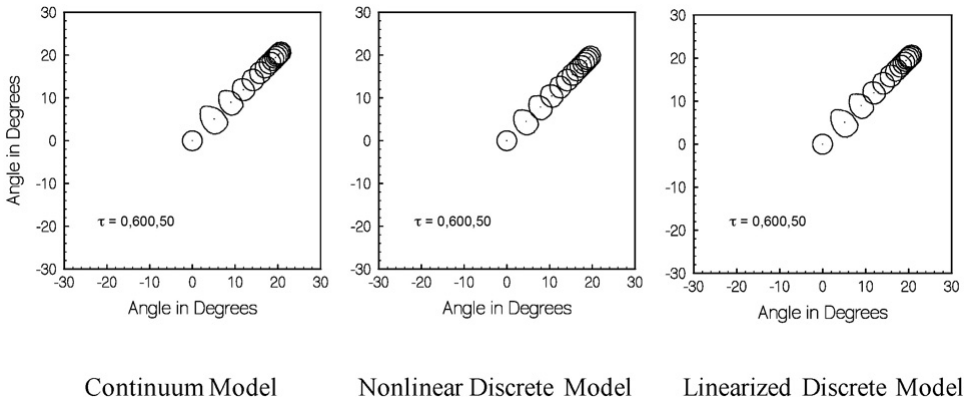


Fig. 4-20. Beam dynamics for hexagonal coupling with $(\theta_0, \varphi_0) = (30\text{ deg}, 45\text{ deg})$ (Reprinted with permission from [44], ©2004 IEEE.)

Now let us revisit in more detail the matter of the steady-state phase distribution in a hexagonally coupled array. We begin by formulating the full nonlinear set of differential equations for such an array. Following Pogorzelski [45], we write for each oscillator,

$$\frac{\partial \varphi_{xy}}{\partial t} = \omega_{tune,xy} - \omega_{ref} - \Delta\omega_{lock} \times \left[\sin(\varphi_{xy} - \varphi_{x-\delta,y}) + \sin\left(\varphi_{xy} - \varphi_{x+\frac{\delta}{2},y+\frac{\sqrt{3}}{2}\delta}\right) + \sin\left(\varphi_{xy} - \varphi_{x+\frac{\delta}{2},y-\frac{\sqrt{3}}{2}\delta}\right) \right] \quad (4.3-12)$$

in which the coupling phase is assumed to be a multiple of 2π and $\delta = 1/\sqrt{3}$, the spacing between coupled oscillators. We have particular interest in the steady state so we set the time derivative equal to zero and get,

$$\frac{\omega_{tune,xy} - \omega_{ref}}{\Delta\omega_{lock}} = \sin(\varphi_{xy} - \varphi_{x-\delta,y}) + \sin\left(\varphi_{xy} - \varphi_{x+\frac{\delta}{2},y+\frac{\sqrt{3}}{2}\delta}\right) + \sin\left(\varphi_{xy} - \varphi_{x+\frac{\delta}{2},y-\frac{\sqrt{3}}{2}\delta}\right) \quad (4.3-13)$$

Recall that the desired phase distribution is given by Eq. (4.3-5). Substituting Eq. (4.3-5) into Eq. (4.3-13), we obtain for the non-perimeter oscillators,

$$\sin\left[D \cos(\varphi_0)\right] + \sin\left[D \cos\left(\varphi_0 + \frac{2\pi}{3}\right)\right] + \sin\left[D \cos\left(\varphi_0 - \frac{2\pi}{3}\right)\right] = 0 \quad (4.3-14)$$

where $D = \frac{2\pi d}{\lambda\sqrt{3}} \sin \theta_0$. Now Eq. (4.3-14) can be rewritten in the form,

$$\sin\left[\frac{D}{2} \cos(\varphi_0)\right] \sin\left[\frac{D}{2} \cos\left(\varphi_0 + \frac{2\pi}{3}\right)\right] \sin\left[\frac{D}{2} \cos\left(\varphi_0 - \frac{2\pi}{3}\right)\right] = 0 \quad (4.3-15)$$

and it is clear that for small D ; that is, small θ_0 , this equation holds approximately true. Moreover, it holds exactly true for $\varphi_0 = \frac{\pi}{6} \pm \frac{n\pi}{3}$ for integer values of n . However, it does not hold true for arbitrary D and φ_0 . Thus, we conclude that no possible detuning of the perimeter oscillators can result in a planar aperture distribution for azimuth angles other than $\varphi_0 = \frac{\pi}{6} \pm \frac{n\pi}{3}$.

Pogorzelski noted, however, that if one postulates a phase distribution of the form,

$$\varphi(x, y) = -\frac{2\pi d}{\lambda} \times \left[\left(x - \frac{N}{\sqrt{3}} \right) \sin \theta_0 \cos \varphi_0 + y \sin \theta_0 \sin \varphi_0 \right] \pm \Delta\varphi_{xy} \quad (4.3-16)$$

in which the ambiguous sign denotes alternation from one oscillator to its neighbor, an exact solution for the perimeter detuning that will produce it is possible provided $\Delta\varphi_{xy}$ is set to the proper value. Substituting Eq. (4.3-16) into Eq. (4.3-13) yields for the non-perimeter oscillators,

$$\begin{aligned} \sin \left[2\Delta\varphi_{xy} - D \cos(\varphi_0) \right] + \sin \left[2\Delta\varphi_{xy} - D \cos \left(\varphi_0 + \frac{2\pi}{3} \right) \right] \\ + \sin \left[2\Delta\varphi_{xy} - D \cos \left(\varphi_0 - \frac{2\pi}{3} \right) \right] = 0 \end{aligned} \quad (4.3-17)$$

and solving for $\Delta\varphi_{xy}$, we obtain,

$$\Delta\varphi_{xy} = \frac{1}{2} \tan^{-1} \left(\frac{Num}{Den} \right) \quad (4.3-18)$$

where,

$$\begin{aligned} Num = \sin \left[D \cos(\varphi_0) \right] + \sin \left[D \cos \left(\varphi_0 + \frac{2\pi}{3} \right) \right] \\ + \sin \left[D \cos \left(\varphi_0 - \frac{2\pi}{3} \right) \right] \end{aligned} \quad (4.3-19)$$

$$\begin{aligned}
 Den = \cos \left[D \cos(\varphi_0) \right] + \cos \left[D \cos \left(\varphi_0 + \frac{2\pi}{3} \right) \right] \\
 + \cos \left[D \cos \left(\varphi_0 - \frac{2\pi}{3} \right) \right]
 \end{aligned}
 \tag{4.3-20}$$

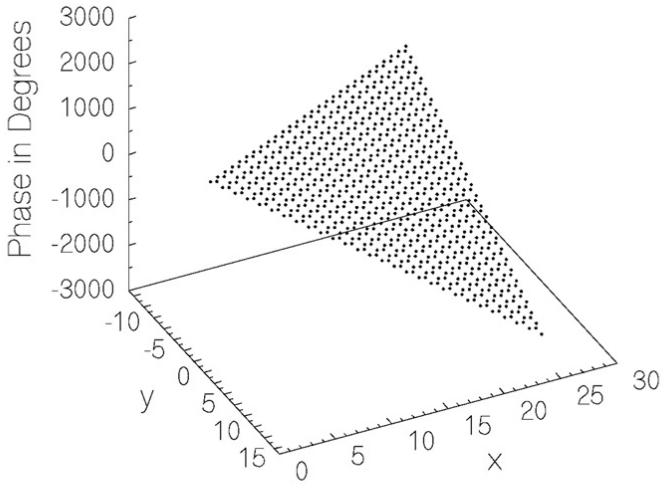
Finally substituting Eq. (4.3-16) with Eq. (4.3-18) into Eq. (4.3-13) yields the perimeter detuning required to produce this non-planar phase distribution. The result is,

$$\begin{aligned}
 \Delta\Omega_{tune} \Big|_{x=y\sqrt{3}} &= -\sin \left[\frac{2\pi d}{\lambda\sqrt{3}} \sin \theta_0 \cos \left(\varphi_0 - \frac{2\pi}{3} \right) - 2\Delta\varphi_{xy} \right] \\
 \Delta\Omega_{tune} \Big|_{x=-y\sqrt{3}} &= -\sin \left[\frac{2\pi d}{\lambda\sqrt{3}} \sin \theta_0 \cos \left(\varphi_0 + \frac{2\pi}{3} \right) - 2\Delta\varphi_{xy} \right] \\
 \Delta\Omega_{tune} \Big|_{x=(3N-1)\sqrt{3}/6} &= -\sin \left[\frac{2\pi d}{\lambda\sqrt{3}} \sin \theta_0 \cos(\varphi_0) - 2\Delta\varphi_{xy} \right]
 \end{aligned}
 \tag{4.3-21}$$

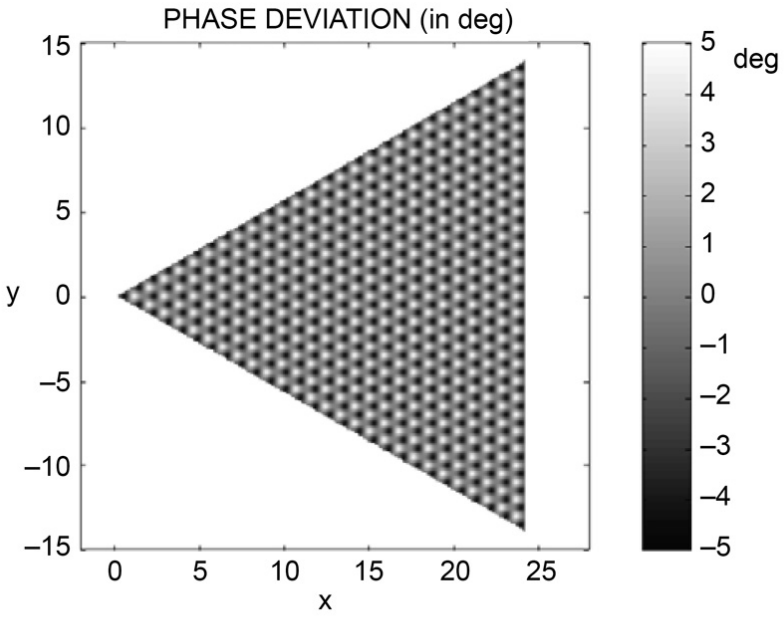
for the edge elements and

$$\begin{aligned}
 \Delta\Omega_{tune} \left(\frac{(3N-1)\sqrt{3}}{6}, \frac{(N-1)}{2} \right) &= \\
 -\sin \left[\frac{2\pi d}{\lambda\sqrt{3}} \sin \theta_0 \cos \left(\varphi_0 + \frac{2\pi}{3} \right) - 2\Delta\varphi_{xy} \right] \\
 \Delta\Omega_{tune} \left(\frac{(3N-1)\sqrt{3}}{6}, -\frac{(N-1)}{2} \right) &= \\
 -\sin \left[\frac{2\pi d}{\lambda\sqrt{3}} \sin \theta_0 \cos \left(\varphi_0 - \frac{2\pi}{3} \right) - 2\Delta\varphi_{xy} \right] \\
 \Delta\Omega_{tune} \left(\frac{1}{\sqrt{3}}, 0 \right) &= -\sin \left[\frac{2\pi d}{\lambda\sqrt{3}} \sin \theta_0 \cos(\varphi_0) - 2\Delta\varphi_{xy} \right]
 \end{aligned}
 \tag{4.3-22}$$

for the corner elements. Because of Eq. (4.3-17), the sum of these detunings is always zero so that the ensemble frequency of the array remains constant. Figure 4-21 shows a typical phase distribution for such an array. Figure 4-21(a) shows the phase distribution, and Fig. 4-21(b) shows the deviation, ± 4.67 deg, from planar.



(a) Phase Distribution



(b) Deviation

Fig. 4-21. Phase distribution for $(\theta_0, \varphi_0) = (22.3 \text{ deg}, 57 \text{ deg})$ with $d = \lambda$ showing (a) phase distribution and (b) deviation from planar. (Reprinted with permission [44], ©2005 IEEE.)

One would perhaps expect that such a phase aberration would result in a decrease in gain. However, as discussed in detail in Ref. [45], this is typically not the case. The power that would have been radiated by a planar phase distribution is partially shifted by the phase alternation into the invisible region. Thus, this part is not radiated, and the power input to the antenna is decreased by the same amount. As a result, the directivity is unaffected by the phase alternation! The only circumstance resulting in a decrease in the gain is when the combination of element spacing and steering angle results in one or more grating lobes in the visible region. Analytical estimation of this effect is discussed in Ref. [45].

Finally, we remark that a planar steady-state phase distribution is of course attainable if one is willing to detune all of the oscillators in the hexagonally coupled array. This would require that alternate oscillators be detuned in opposite directions in frequency by an amount that depends on the scan angle.

4.4 Conclusion

In this chapter we have discussed a variety of coupling topologies for planar arrays, and we have shown that the continuum model can be used to describe the dynamic behavior of the phase distribution over these arrays. By this means we have demonstrated that beam-steering can be accomplished by detuning the perimeter oscillators or in the Cartesian case by injection locking them to external signals. Beam-steering by external injection in the triangular case was not treated but appears to be possible, though the analysis may become somewhat more challenging.

In the next chapter we point out that all of the preceding results are fundamentally non-causal in that the response begins immediately upon application of the detuning or phase shift of the external locking signal regardless of the physical separation of the cause and effect. A modified formulation is proposed to render the solutions causal.

